TSG-RAN WG4 meeting #57 AH **R4-110455**
Austin, TX, USA 17 – 21 December 2011

Source: ETS-Lindgren

Title: Site Validation of an Anechoic Chamber Based MIMO OTA System

Agenda item: 6.2

Document for: Discussion

---

1 Introduction

In evaluating methodologies for over-the-air (OTA) testing of MIMO devices, it's important to look at potential sources of error and attempt to determine their impact on measurement results. Existing SISO methods for evaluating TRP/TRS in an anechoic chamber include a ripple test method for evaluating the quality of the test volume and its impact on the measurement uncertainty [1]. Similar methods are needed for evaluating the simulated RF environment created for MIMO OTA testing. While the existing ripple test methodologies can certainly be used and enhanced to evaluate the performance of an anechoic chamber used for MIMO OTA testing, additional validation tests are required to determine the ability of a given system to produce the target RF environment. This paper presents the results of several system validation tests performed on an RF environment simulation system comprised of an array of transmit antennas in an anechoic chamber, connected to a bank of radio channel emulators.

2 System Configuration

The basic design of the environment simulation system has been well documented elsewhere [2]-[9]. The system used for these tests contained sixteen dual-polarized downlink antennas in an evenly spaced circular array (22.5° spacing) with a 2.0 m range length, connected to two eight-port channel emulators, allowing dual polarized operation with eight antennas, or a single polarized operation with all sixteen antennas. The basic concept is illustrated in Figure 1, while the actual system being evaluated is show in Figure 2.

All tests were performed at 2112.4 MHz to a radius of 0.5 m (1.0 m diameter) in order to evaluate the test volume used for the MIMO OTA round robin testing. This test region covered multiple wavelengths and a significant fraction of the 2.0 m range length in order to evaluate the impact of these factors.

A ripple test was performed on the system to evaluate the chamber performance itself. The maximum ripple was less than +/- 0.5 dB (1.0 dB peak-to-null). This represents an extremely high performance level for the chamber absorber treatment, etc.

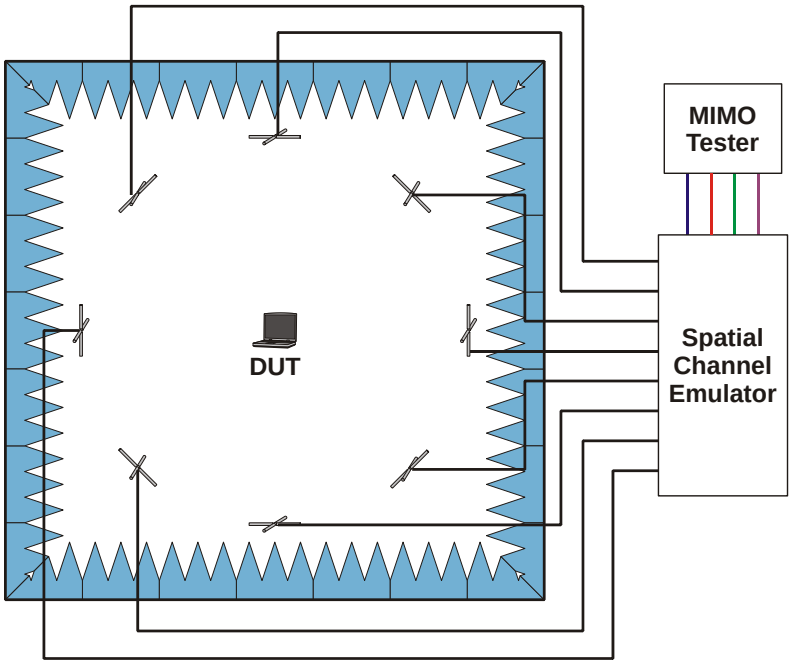

Figure 1. An array of antennas in an anechoic chamber simulate reflections from different directions around the DUT. A channel emulator is used to simulate the propagation of communication signals through a modeled environment between the test equipment and the DUT.

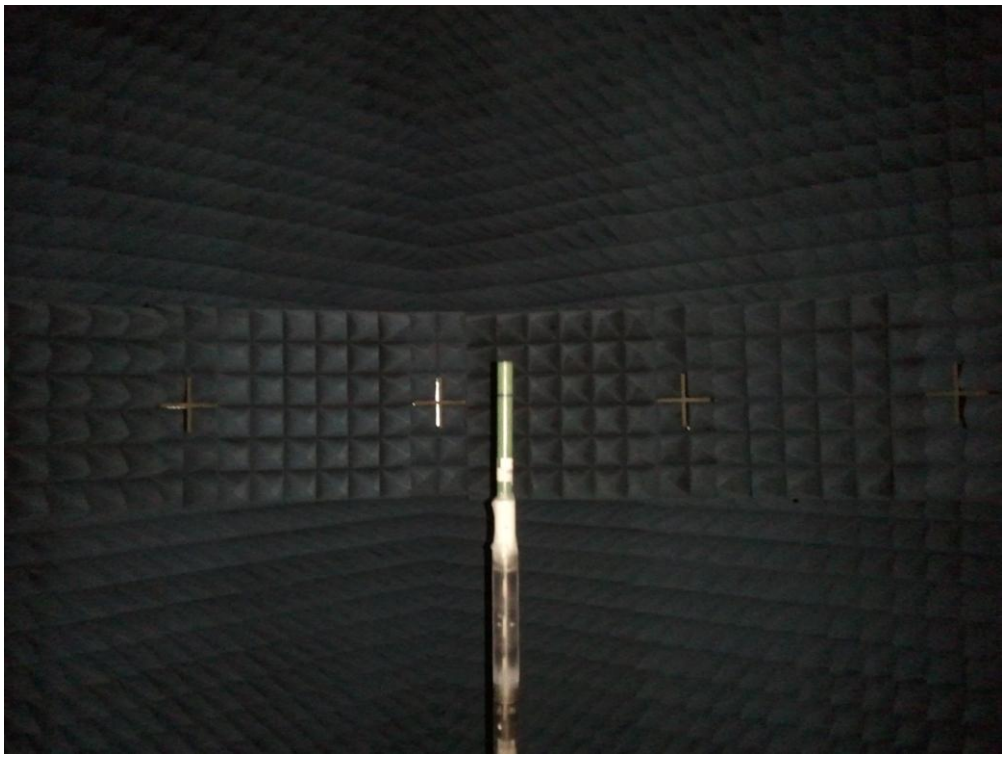

Figure 2. Photo of the sixteen antenna array with a 2.0 m range length, showing the sleeve dipole used to probe the test volume.

3 Spatial Field Mapping

By phase calibrating the system in addition to a magnitude calibration, the expected field structure can be evaluated. Once all sources in the array have the same phase and magnitude relationship with a dipole placed in the exact center of the test volume, the contributions from a constant tap channel model can be expected to add in phase in the center of the test volume. The expected field structure generated by any given array symmetry can be readily calculated for comparison to that generated by the system. Figure 3 shows the eight-fold symmetry produced by an array of eight antennas evenly distributed around the center in the far field.

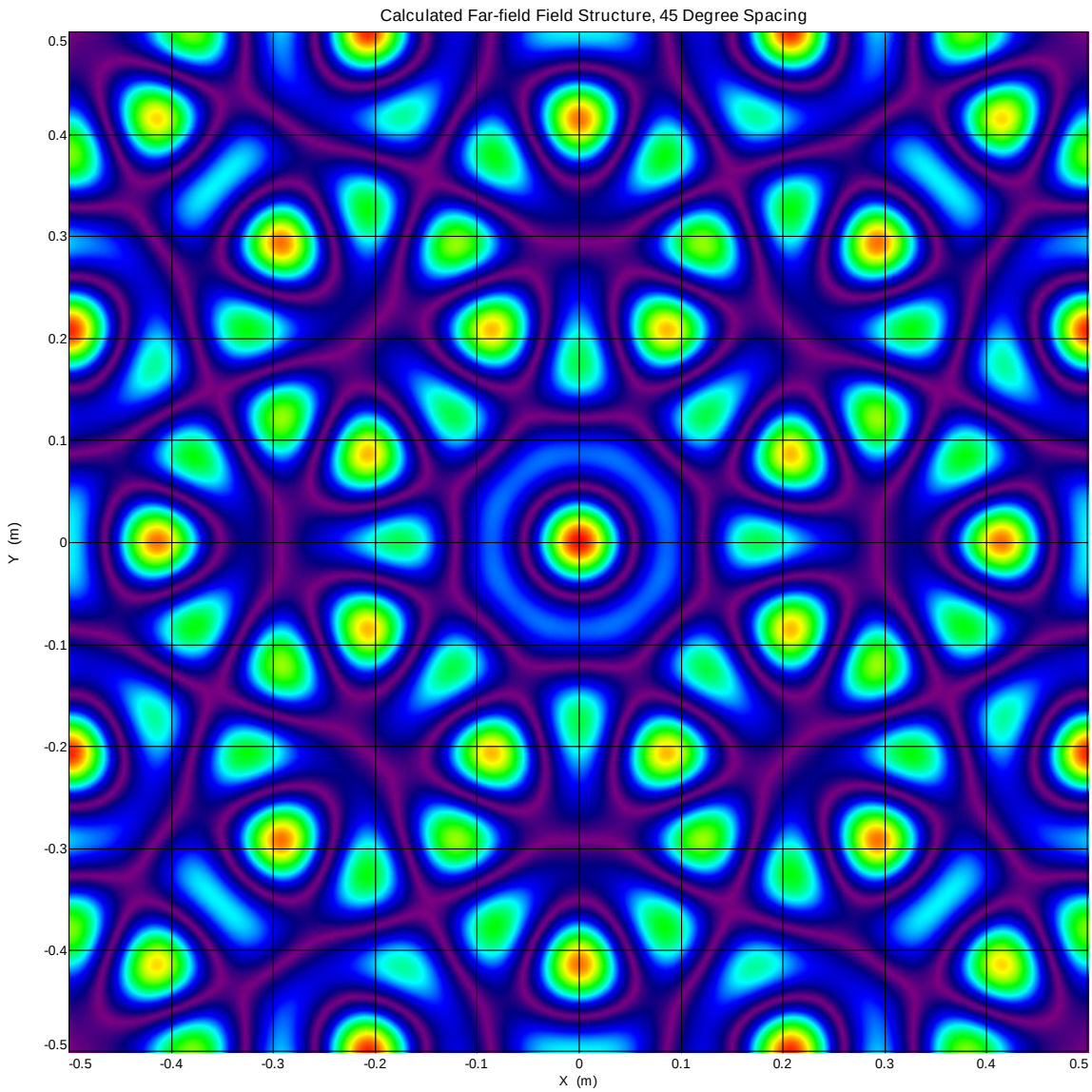

Figure 3. Calculated field structure from a vertically polarized eight antenna array in the far field.

For comparison, the field structure from a continuous boundary condition in free-space is given in . The impact of the 45° resolution of the antenna elements becomes clear in the form of

an eight-fold symmetry after about one-half wavelength from the center of the test volume. In the ideal environment, the target field structure for this test would resemble the ripple from a single drop of water on a perfectly smooth pond. The same drop of water in the center of a perfectly round container would result in a reflected wave pattern matching that shown in Figure 4. If instead, eight sticks were evenly spaced around the drop, the reflection pattern produced would show the complex interference pattern as in Figure 3. Thus, the field mapping provides an effective evaluation of the boundary condition produced by the system.

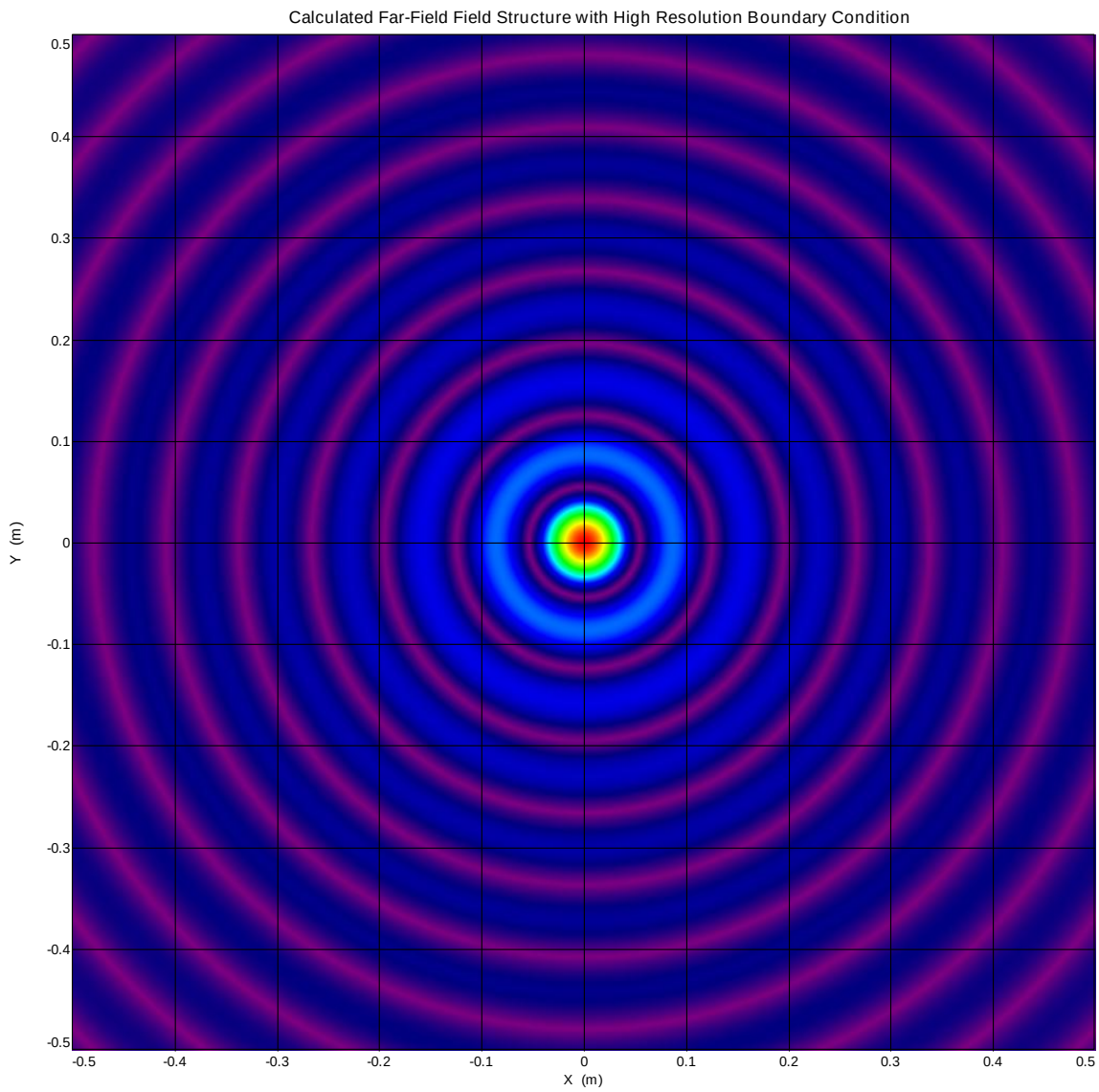

Figure 4. Calculated field structure from a vertically polarized high resolution far field boundary condition.

The vertically polarized field structure of the test system was evaluated using a vertically polarized sleeve dipole. The field structure was mapped every 1.0 cm in radius and every 1.0 degree in angle, giving a tangential resolution of ~0.9 cm at the edge of the test volume. The results seen in Figure 5 do a good job of replicating the expected structure in the middle of the

test volume, but show only a passing resemblance to the previous picture in the outer 25 cm of radius.

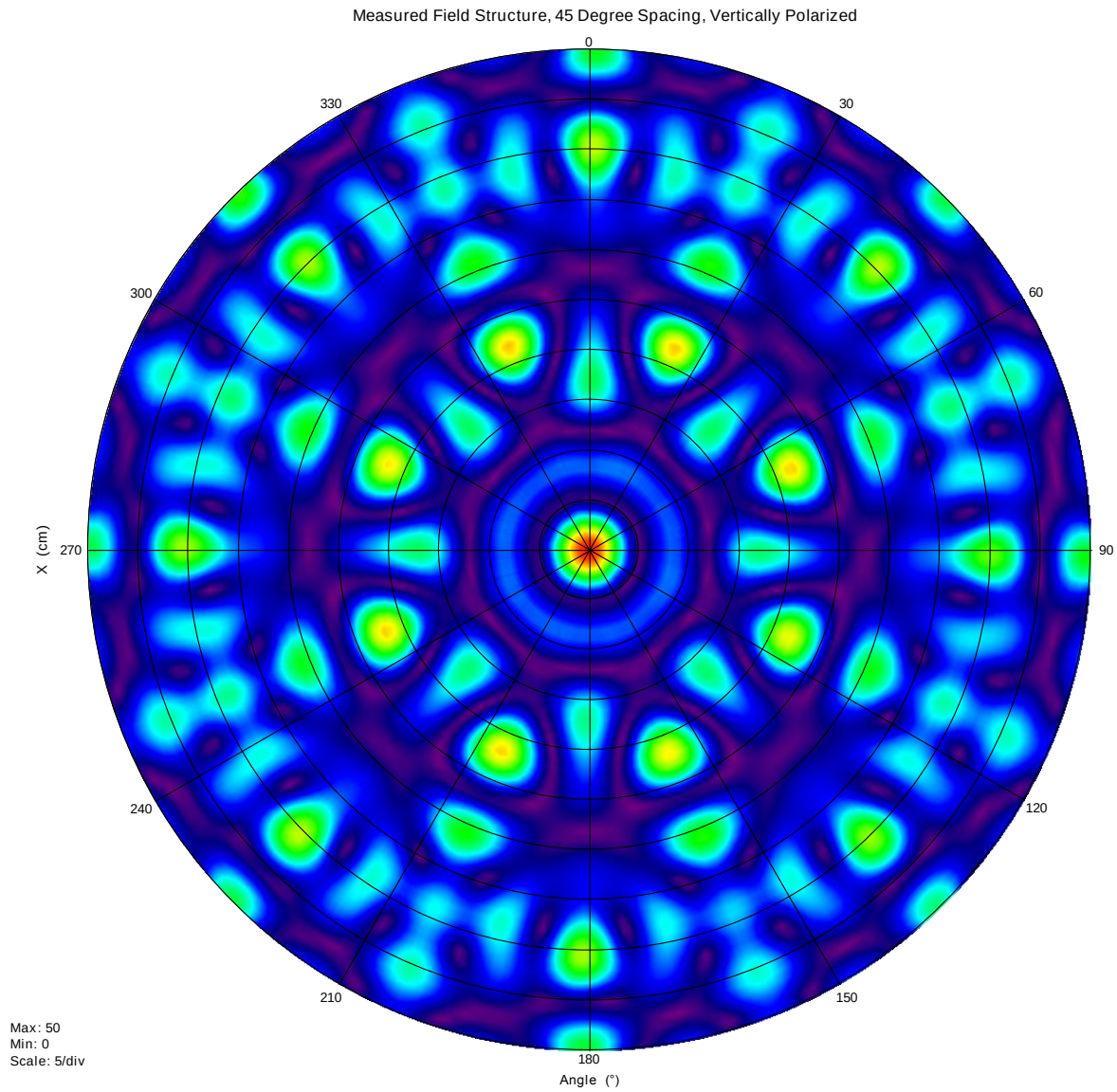

Figure 5. Measured field structure from an eight antenna array with a 2.0 m radius.

While the performance in this region is generally not of interest due to the expected deviation from the ideal conditions of a free-space environment with a continuous boundary condition (Figure 4), it's still important to understand the cause of any apparent deviations from the expected behavior. In this case, the deviation can be easily explained by calculating the expected field structure from a dipole array placed at a 2.0 m radius as shown in Figure 6. The main source of the deviation from the far field structure is clearly caused by the 1/r relationship with the array antennas, where the signal from a single source antenna can vary by +2.5/-2 dB at the edge of the test volume from that in the center. In this case, it's also apparent that, after angular resolution of the sensors, range length is the principal contribution to the quality of the test

volume. The impact of the beam patterns of the horns used for this array is indistinguishable from that of the dipole pattern used to calculate the expected field volume.

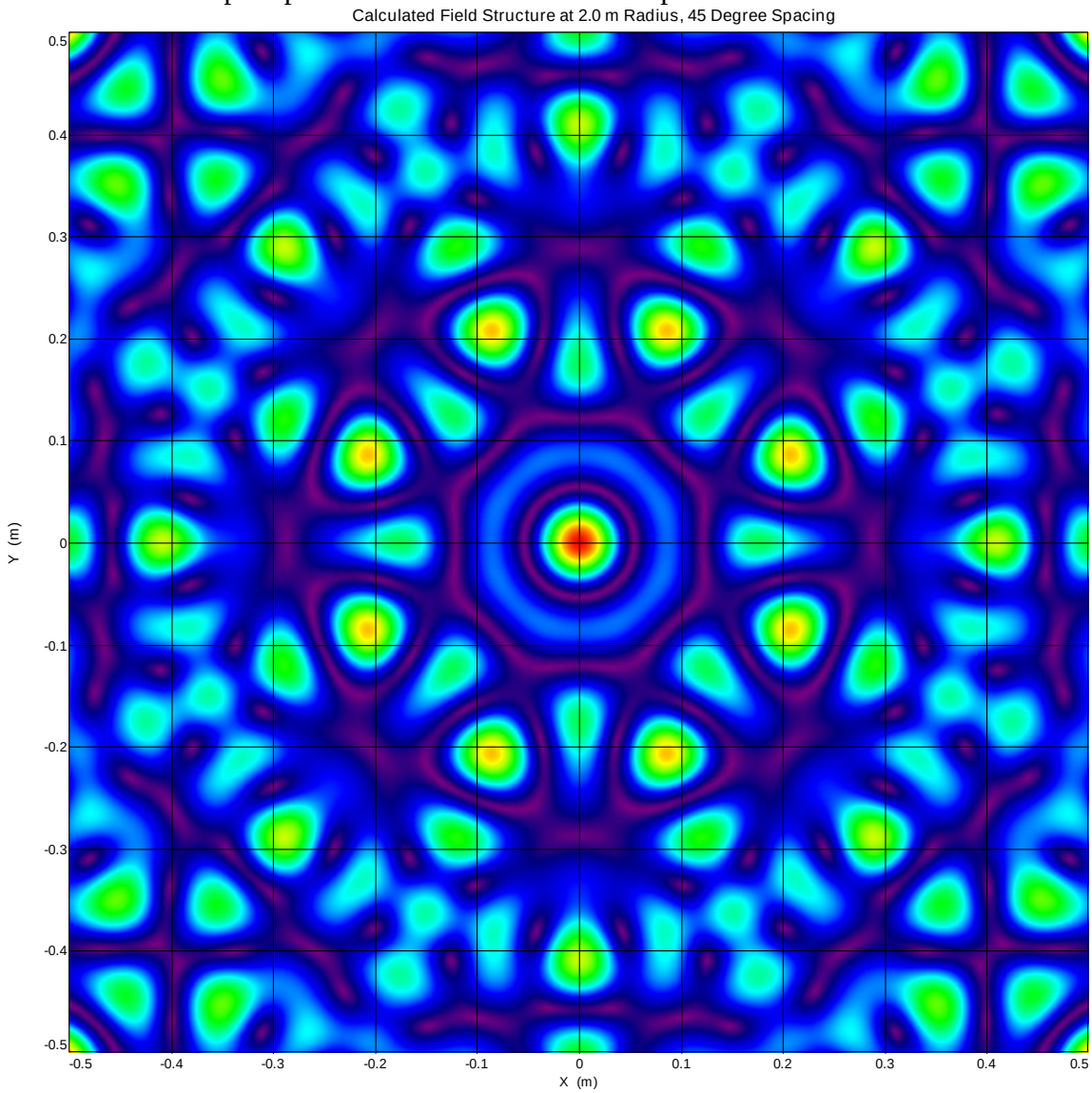

Figure 6. Calculated field structure from an eight antenna dipole array with a 2.0 m radius.

For horizontal polarization, matters are slightly different. Using a magnetic loop antenna that has a horizontally polarized omnidirectional pattern in the horizontal plane (i.e. a magnetic dipole instead of an electric dipole) the field mapping in Figure 7 looks much like that in Figure 6. This makes sense, since each source antenna is phase and magnitude adjusted to produce the same signal at the port of the loop antenna so that they all sum in phase in the very center of the test volume. However, this behavior is peculiar to the properties of the loop antenna itself, and do not represent the actual field structure in the test volume. This can be seen by considering the use of a horizontally polarized horn to calibrate each antenna in the array. As the horn is rotated to face an antenna on the opposite side of the array, its polarization is changed by 180° relative to

the first antenna. Thus, the expected field structure for a phase calibrated horizontal array is to have a null in the very center of the test volume as shown in Figure 8, since opposite antennas cancel each other out, rather than adding like they do for vertical polarization. It is not physically possible to create a condition where opposite antennas add without producing an un-realizable null somewhere else along the angular distribution in question.

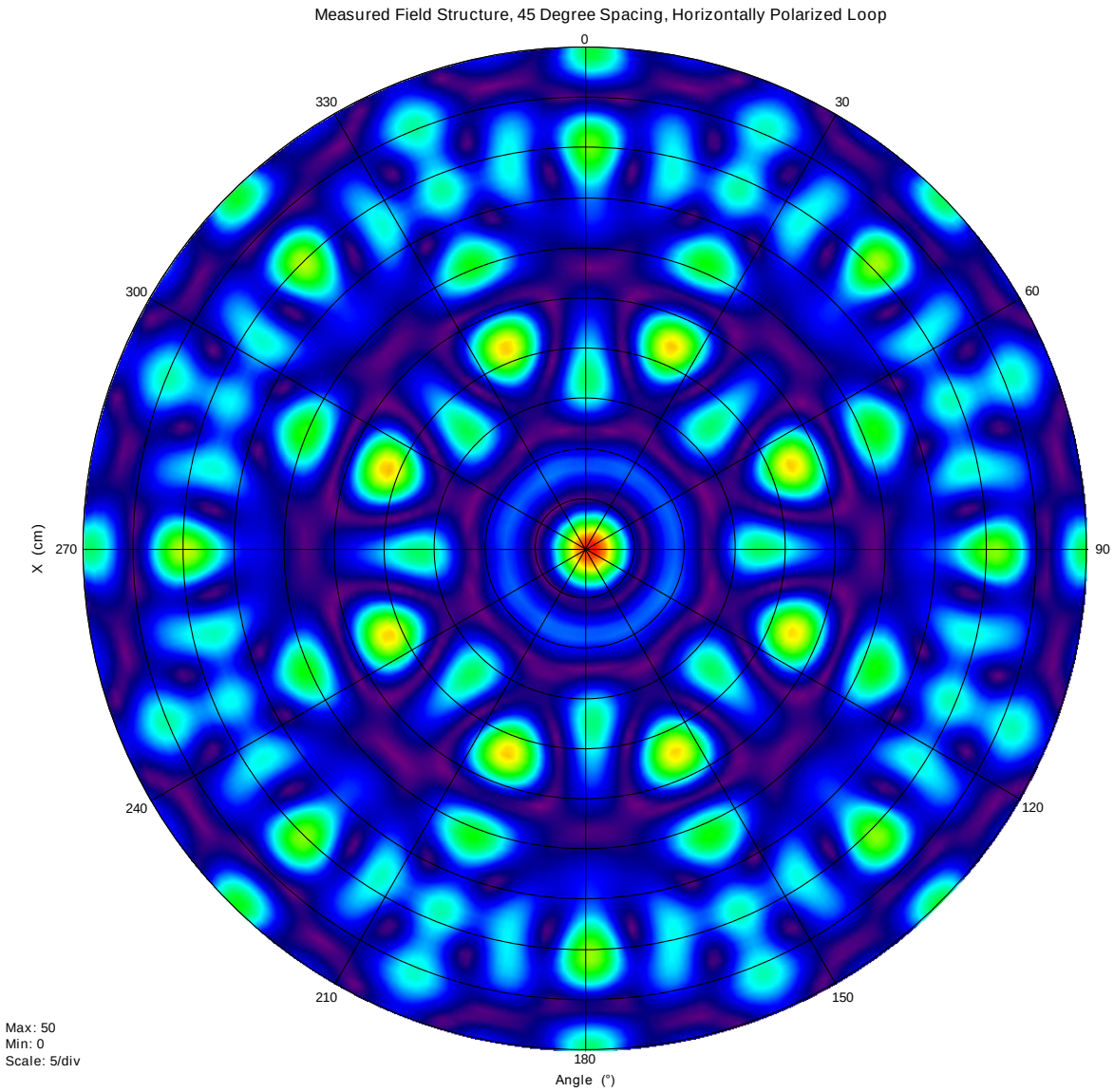

Figure 7. Measured horizontal polarization map using an omnidirectional loop (magnetic dipole) for an eight antenna array with a 2.0 m radius.

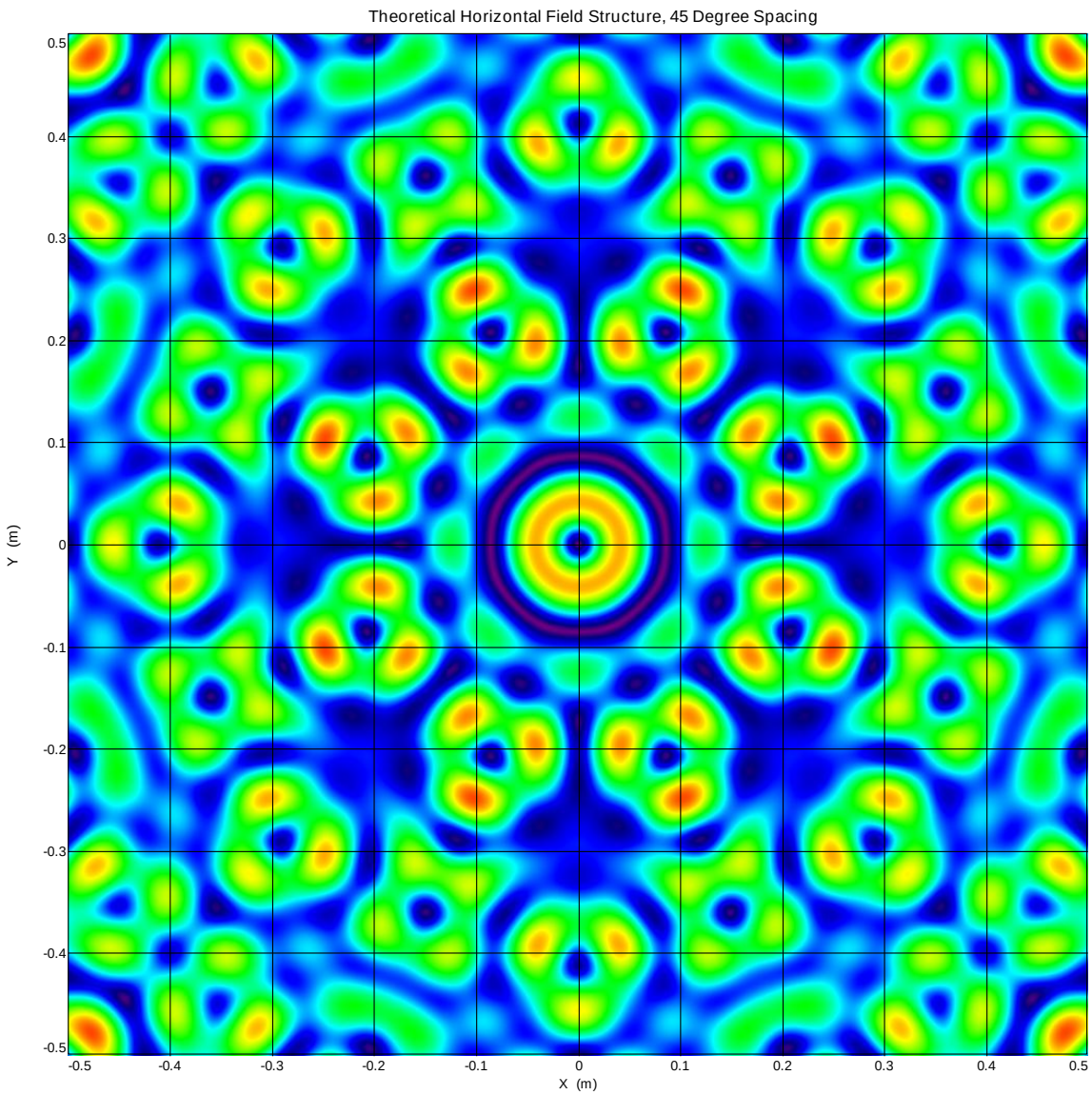

Figure 8. Expected field structure for a horizontally polarized eight antenna array. Note the null in the center of the test volume caused by cancellation from the opposite side of the array.

In order to measure this field structure as shown, it's necessary to use an electric dipole and evaluate two orthogonal horizontal components at each point in the test volume. Figure 10 and Figure 11 show the two orthogonal field components, one oriented longitudinally along the radial positioner axis and the other oriented perpendicular to the first. Figure 9 shows the vector sum of the magnitudes of these two components. Allowing for the slight misalignments involved in the crude Styrofoam fixture used to mount the dipole horizontally, the expected field structure can be readily identified in the resultant pattern.

Given the relative ease of using the magnetic loop for evaluating the horizontal field structure of a system, the additional complexity of this approach seems unwarranted. However, the

magnetic dipole does suffer from the limitation that it is inherently narrow band, maintaining symmetry over only a few MHz of bandwidth. Provided this validation is only needed for a few frequencies, this should not be a major limitation. However, if a more detailed frequency mapping is required, the electric dipole alternative may be superior. One other advantage of using the electric dipole to evaluate both polarizations is that the same absolute reference can then be applied. While not necessary for the purpose of this field mapping exercise, this becomes important for evaluating/validating the XPR generated by a chosen channel model.

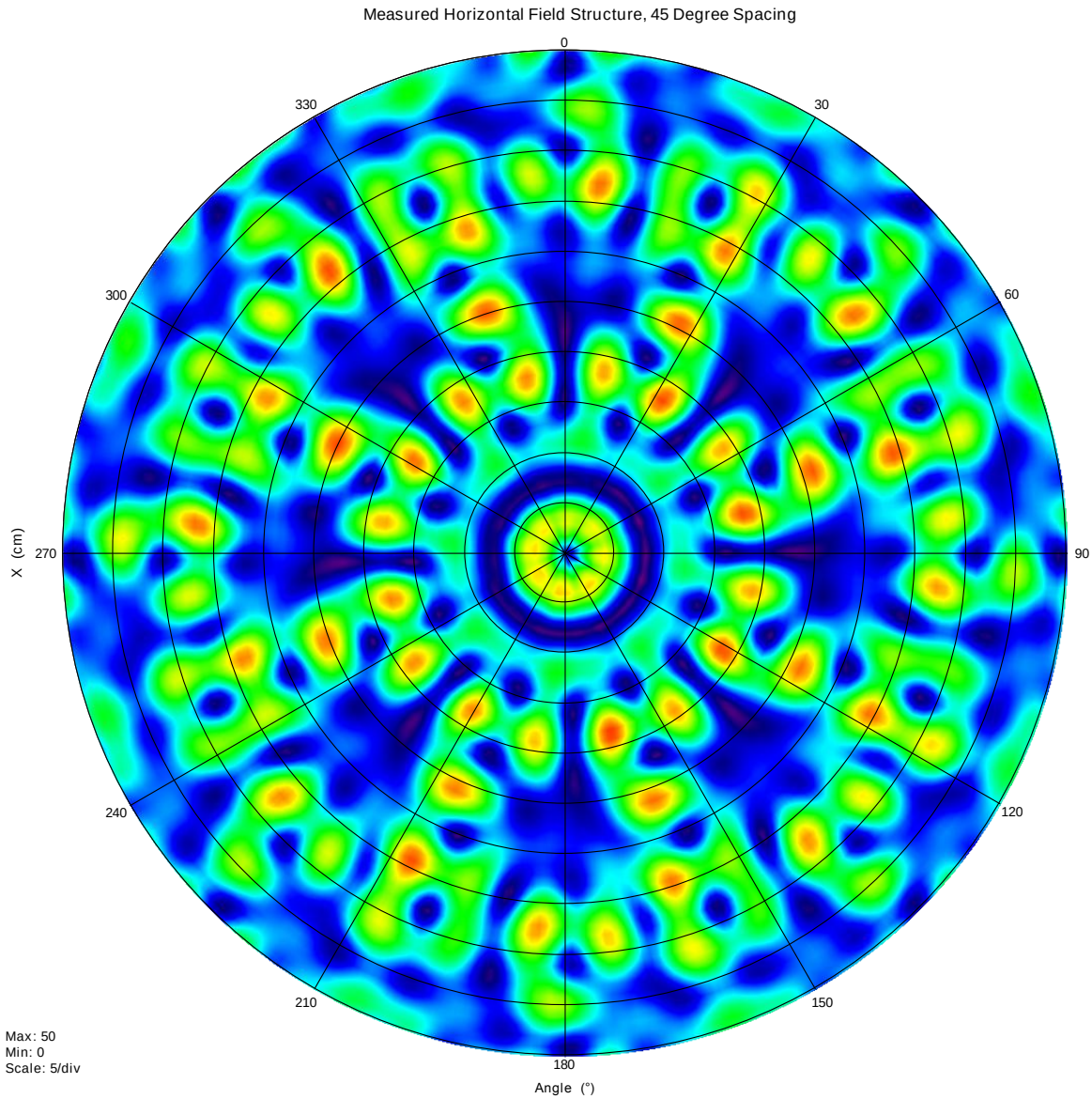

Figure 9. Sum of two measured orthogonal horizontal field components for an eight antenna array with a 2.0 m radius.

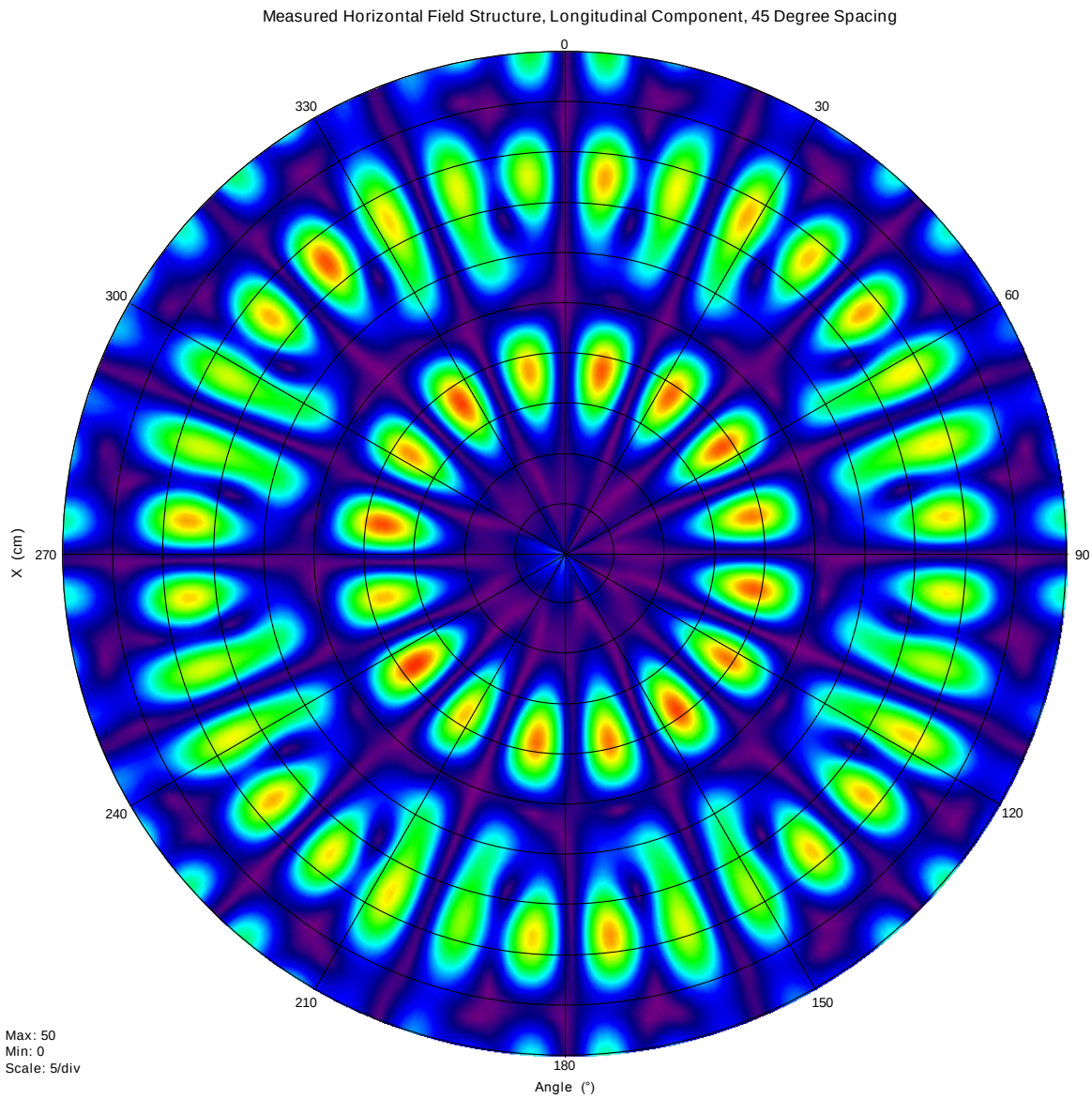

Figure 10. Measured horizontal field component with the dipole oriented radially in the test volume for an eight antenna array with a 2.0 m radius.

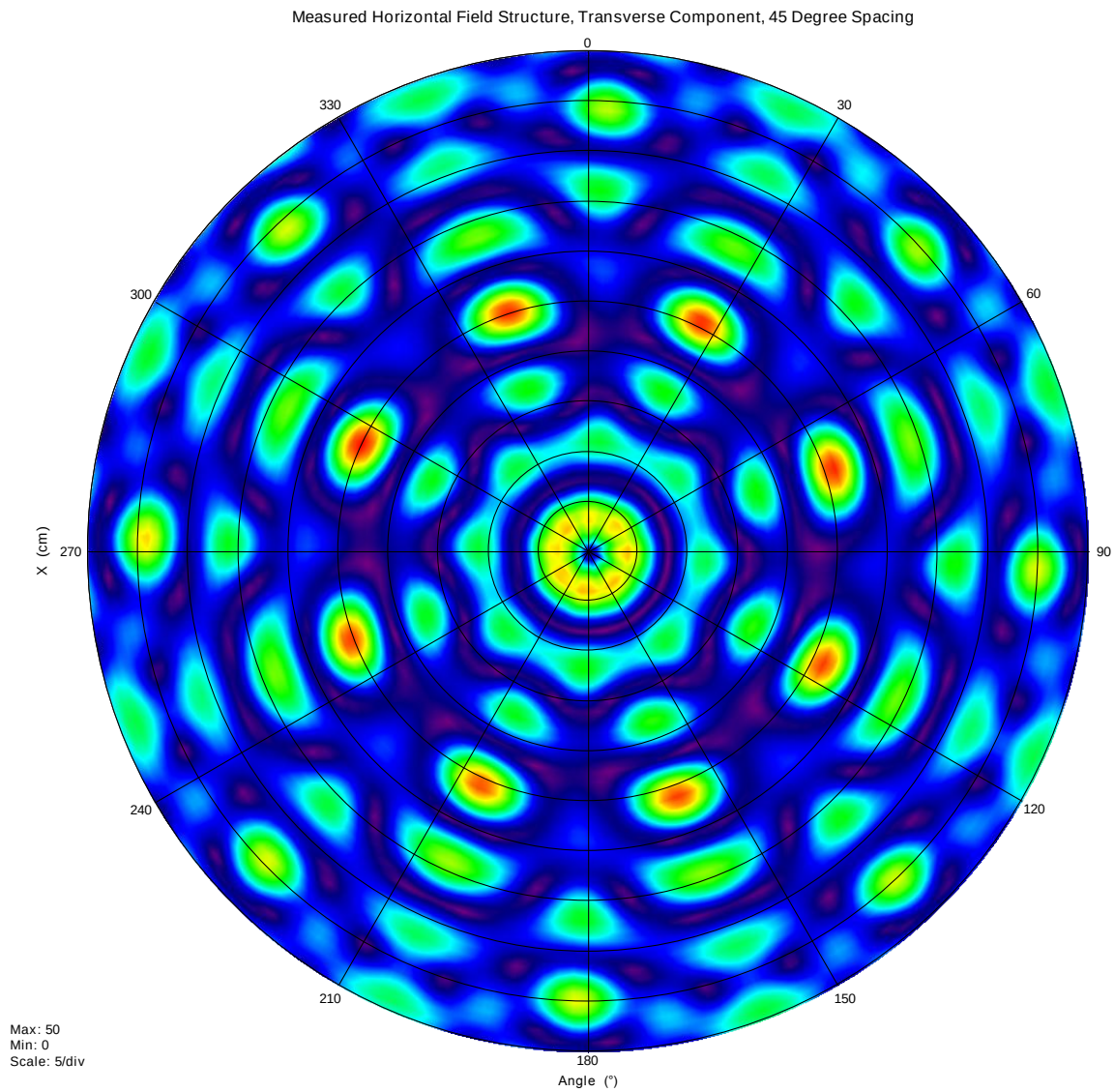

Figure 11. Measured horizontal field component with the dipole oriented tangentially in the test volume for an eight antenna array with a 2.0 m radius.

The system was also evaluated for 16 vertically polarized antennas (22.5° spacing) to determine the increase in usable test volume. As shown in Figure 12, the useable test volume is considerably larger before finally breaking up into an interference pattern. Figure 13 and Figure 14 show the measured result. The overall pattern clearly matches, although an undetected problem with the system setup resulted in compression of the peaks when the additional 6 dB of signal was added from doubling the array size.

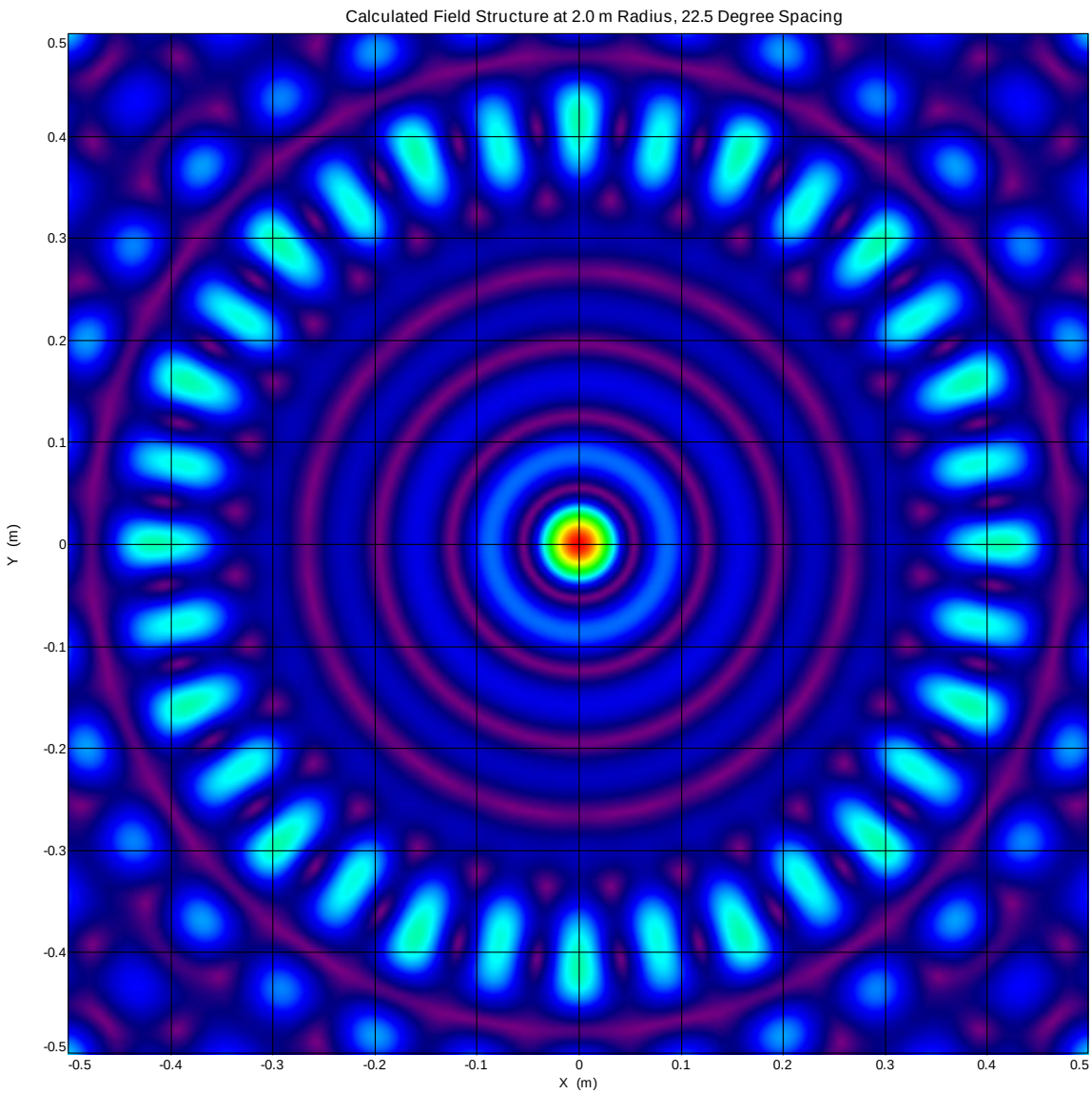

Figure 12. Expected field structure for a vertically polarized sixteen antenna dipole array.

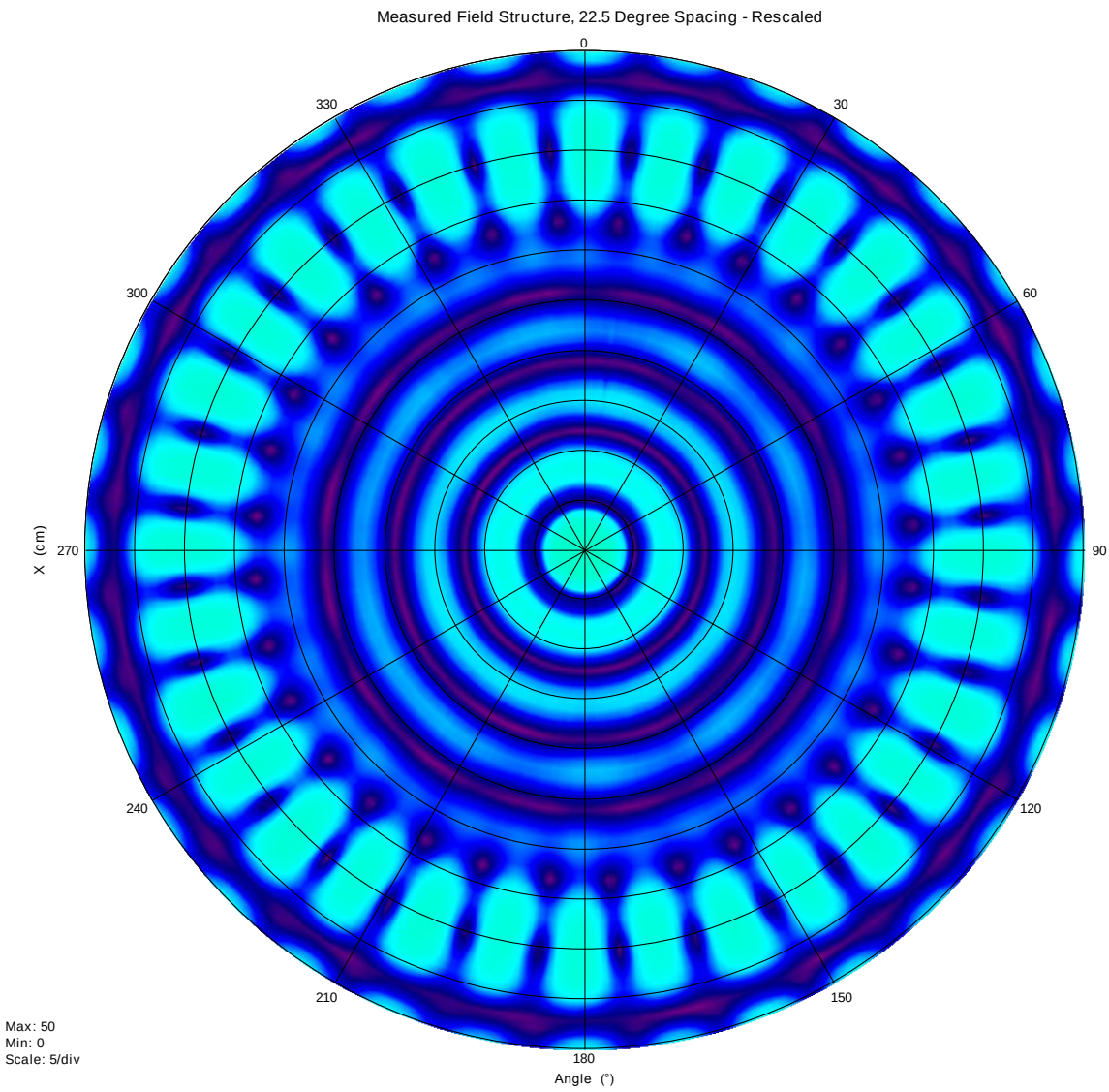

Figure 13. Measured vertically polarized field structure for sixteen antenna array with a 2.0 m radius. Data is scaled to make lower portion of curves align with reference.

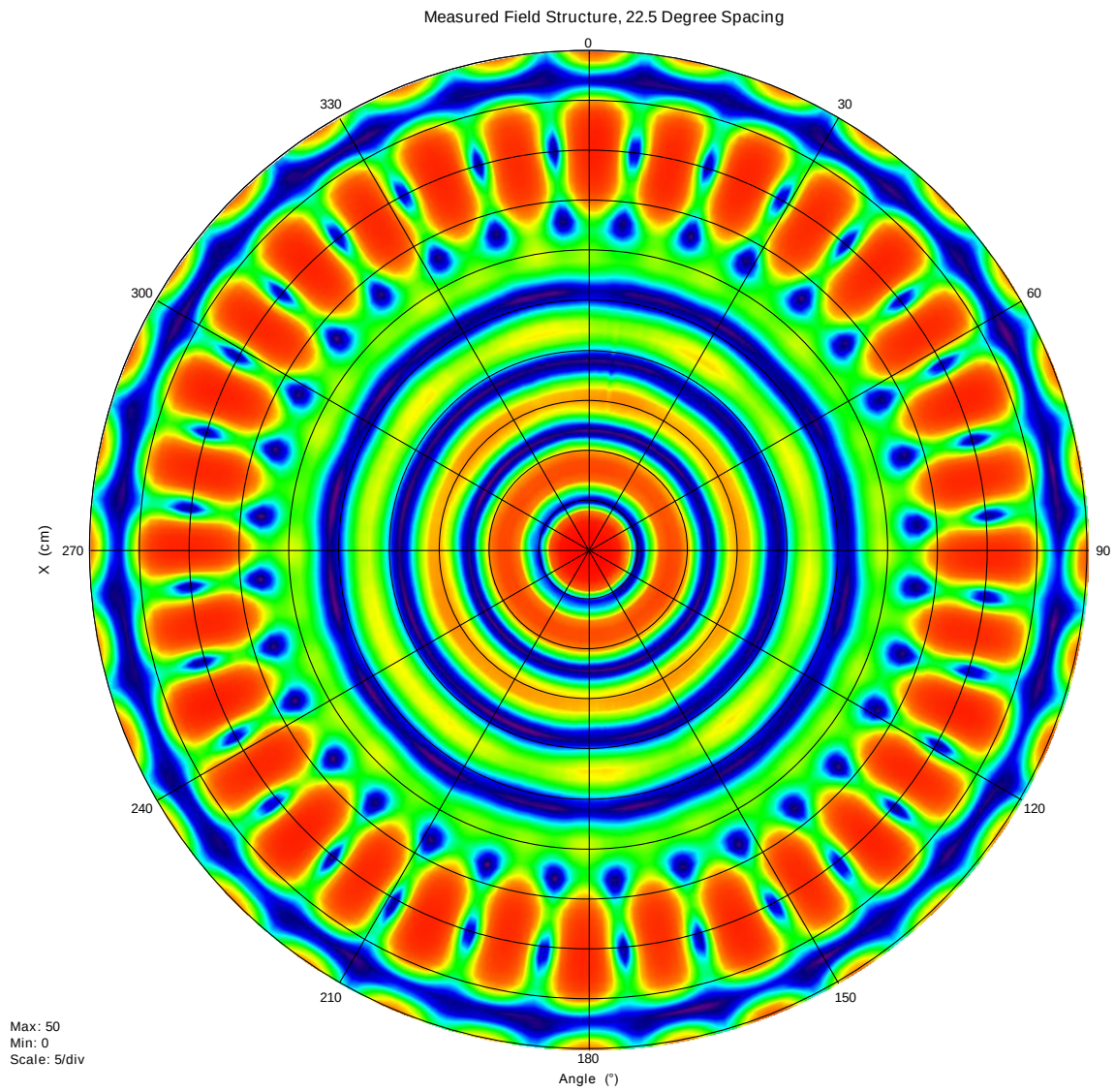

Figure 14. Measured vertically polarized field structure for sixteen antenna array with a 2.0 m radius. Test system was in compression resulting in flattened peaks.

4 Spatial Correlation

In addition to evaluating the quality of the test volume, it's also useful to evaluate the channel emulation capability be performing a spatial correlation test. The spatial correlation test evaluates the ability of the given environment, including the channel model, to produce an uncorrelated test volume. This is different from evaluating the correlation of two antennas placed within that test volume.

For the purpose of this test, a single cluster with a 35° angular spread was used and a single slice through the test volume perpendicular to the direction of the cluster center was evaluated.

Figure 15 shows the measured spatial correlation for the eight antenna (45° resolution) system, and Figure 16 gives the result for the 16 antenna (22.5° resolution). It is interesting to compare these results with that of the field structure measurement as shown in Figure 17 and Figure 18. Figure 19 shows the same data as Figure 18 overlaid on the calculated high resolution field structure. It clearly shows that the correlation begins to increase as the field structure begins to deviate from the ideal. This again illustrates the value of the field mapping method since it provides a full volumetric analysis that is lacking from the correlation based test.

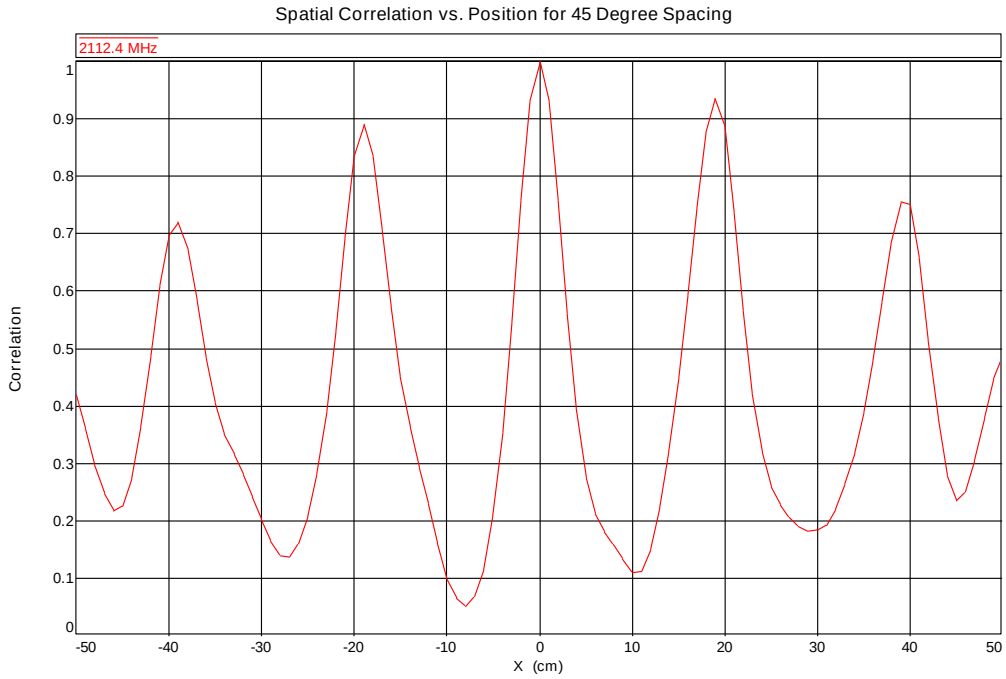

Figure 15. Spatial correlation of a single cluster channel model for the eight antenna ring.

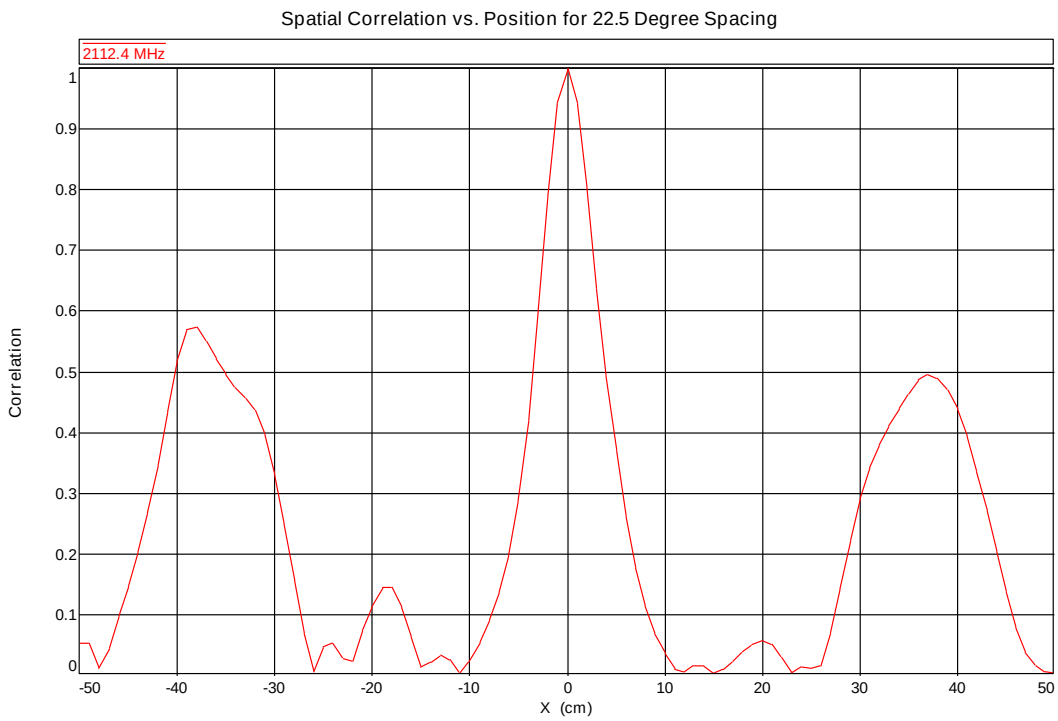

Figure 16. Spatial correlation of a single cluster channel model for the sixteen antenna ring.

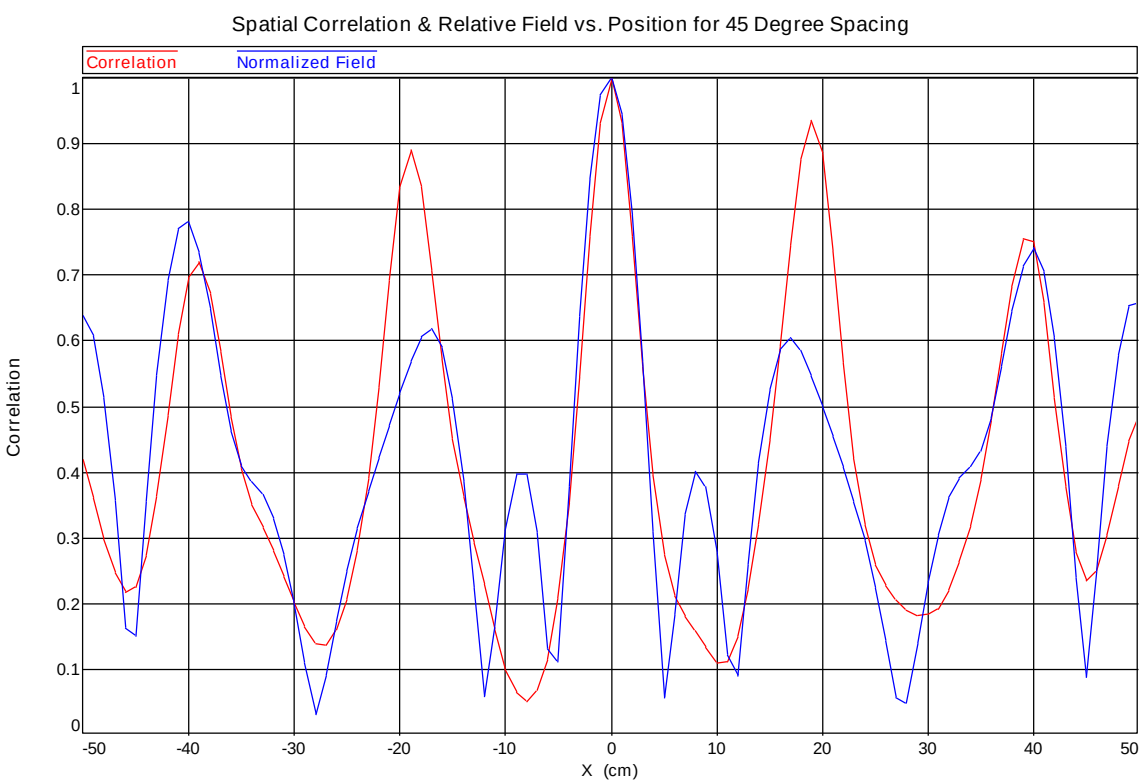

Figure 17. Comparison of the field structure and correlation for the eight antenna ring.

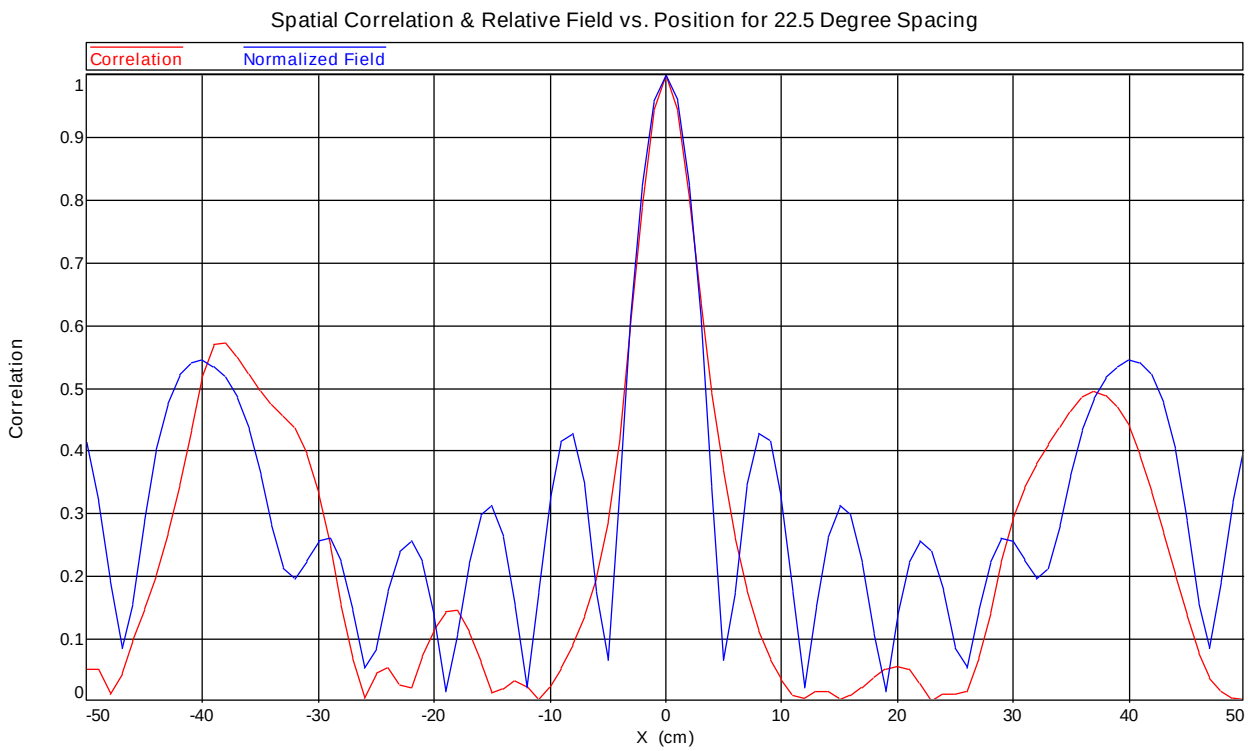

Figure 18. Comparison of the field structure and correlation for the sixteen antenna ring.

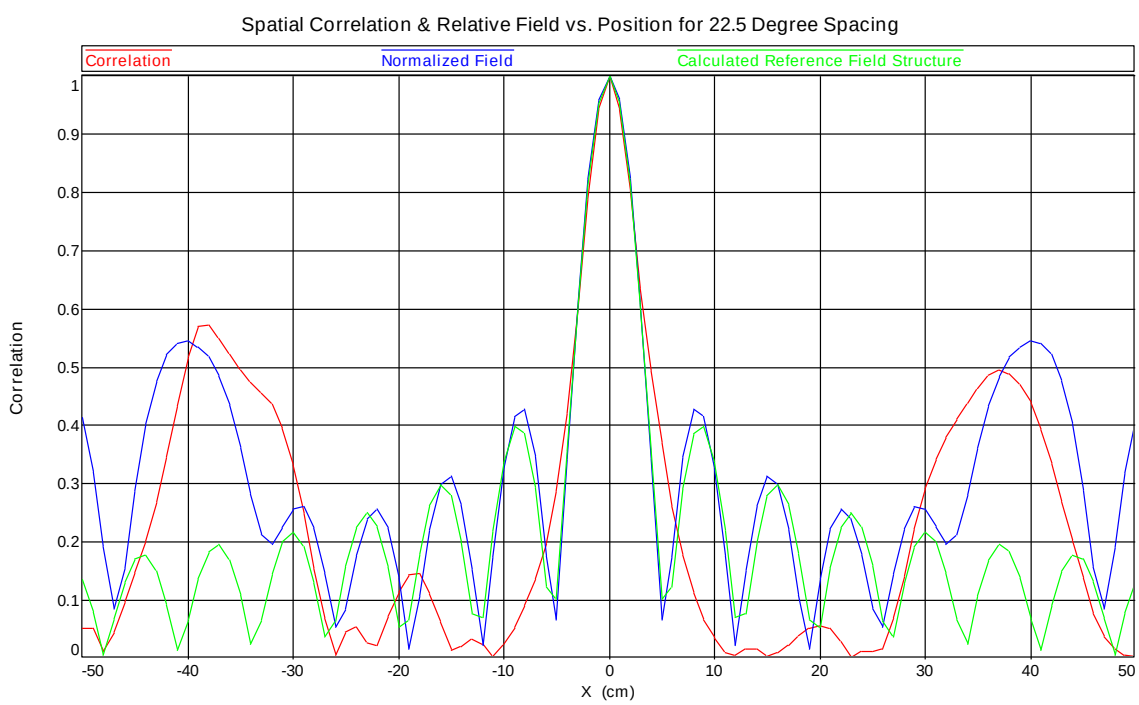

Figure 19. Comparison of the field structure vs. the reference field structure, showing that correlation increases when the measured result starts to deviate from the ideal behavior.

5 Conclusion

A thorough site validation was performed on an anechoic chamber based MIMO OTA test system. In addition to traditional ripple test methods, volumetric field mapping of the test environment and spatial correlation are shown as useful validation methods for evaluating these systems. These techniques will need to be evaluated for inclusion in any resulting MIMO OTA test plan. Additional methods for evaluating XPR and other model specific metrics may also be required.

6 References

[1] *Test Plan for Mobile Station Over the Air Performance, Revision 2.1*, CTIA – The Wireless Association, Washington, D.C., April 2005.

[2] Foegelle, M.D., "Over-the-Air Performance Testing of Wireless Devices with Multiple Antennas," RF Design, February 2006, pp. 44-52.

[3] Foegelle, M.D., "Systems and Methods for Over the Air Performance Testing of Wireless Devices with Multiple Antennas," United States Patent Application Publication 2008/0056340 A1, March 6, 2008.

[4] Foegelle, M.D., "Systems and methods for over-the-air testing of wireless systems," United States Patent Application Publication 2008/0305754 A1, December 11th, 2008.

[5] Foegelle, M.D., "OTA Performance Testing of Wireless Devices with Multiple Antennas," Antenna Measurement Techniques Association (AMTA 2006), PID 524/A06-001.

[6] Foegelle, M.D., "Calibration and Validation of an Anechoic Chamber Based MIMO OTA System," COST 2100 TD(10) 111022, Aalborg, Denmark, June 2010.

[7] Foegelle, M.D., "Creating a Complex Multipath Environment Simulation in an Anechoic Chamber," Microwave Journal, August 2010, Vol 53, No. 8, p 56.

[8] Foegelle, M.D., "A Multipath Environment Simulator for OTA Testing of MIMO and Other Multiple Antenna Technologies", AMTA 2010, PID A10-0114.

[9] R4-102241 "Test Plan for Anechoic Chamber based MIMO OTA methods," Elektrobit, Nokia, ETS-Lindgren, SATIMO, Spirent Communications, Agilent Technologies, Rohde & Schwarz, NTT DOCOMO, LG Electronics